

This work was written as part of one of the author's official duties as an Employee of the United States Government and is therefore a work of the United States Government. In accordance with 17 U.S.C. 105, no copyright protection is available for such works under U.S. Law.

Public Domain Mark 1.0

<https://creativecommons.org/publicdomain/mark/1.0/>

Access to this work was provided by the University of Maryland, Baltimore County (UMBC) ScholarWorks@UMBC digital repository on the Maryland Shared Open Access (MD-SOAR) platform.

Please provide feedback

Please support the ScholarWorks@UMBC repository by emailing scholarworks-group@umbc.edu and telling us what having access to this work means to you and why it's important to you. Thank you.

Monitoring Orbital Precession of EO-1 Hyperion With Three Atmospheric Correction Models in the Libya-4 PICS

Christopher S. R. Neigh, Joel McCorkel, Petya K. E. Campbell, Lawrence Ong, Vuong Ly, David Landis, and Elizabeth M. Middleton

Abstract—Spaceborne spectrometers require spectral-temporal stability characterization to aid in validation of derived data products. Earth Observation 1 (EO-1) began orbital precession in 2011 after exhausting onboard fuel resources. In the Libya-4 pseudoinvariant calibration site (PICS), this resulted in a progressive shift from a mean local equatorial crossing time of $\sim 10:00$ A.M. in 2011 to $\sim 8:30$ A.M. in late 2015. Here, we studied precession impacts to Hyperion surface reflectance products using three atmospheric correction approaches from 2004 to 2015. Combined difference estimates of surface reflectance were $<5\%$ in the visible near infrared (VNIR) and $<10\%$ for most of the shortwave infrared (SWIR). Combined coefficient of variation estimates in the VNIR ranged from 0.025 to 0.095, and in the SWIR it ranged from 0.025 to 0.06, excluding bands near atmospheric absorption features. Reflectances produced with different atmospheric models were correlated (R^2) in VNIR from 0.25 to 0.94 and in SWIR from 0.12 to 0.88 ($p < 0.01$). The uncertainties in all the models increased with a terrain slope up to 15° and selecting dune flats could reduce errors. We conclude that these data remain a valuable resource over this period for sensor intercalibration despite orbital decay.

Index Terms—Atmospheric correction now (ACORN), atmospheric removal program (ATREM), EO-1 Hyperion, fast line-of-sight atmospheric analysis of spectral hypercubes (FLAASH), land surface imaging (LSI), Libya-4, orbital precession, pseudoinvariant calibration site (PICS), surface reflectance, time-series analysis.

I. INTRODUCTION

ANALYSIS of Earth Observation 1 (EO-1) Hyperion high spectral resolution imagery ($0.4\text{--}2.5\ \mu\text{m}$) is needed to link data products for cross-calibration [1]. These data could

be used for multispectral data replication, or for on orbit cross-calibration among satellite instruments [1]–[3] to create a land surface imaging (LSI) virtual constellation approach of merging similar but disparate satellite records. Estimating trends in Hyperion products due to precession could support future LSI studies, as the LSI virtual constellation concept is only viable if the stability of constituents and associated uncertainties is known. EO-1 Hyperion currently has the longest spaceborne spectrometer record extending to more than 15 years. Launched in 2000, EO-1 was a one-year technology demonstration mission, but it was extended multiple times [4]. It has been useful for testing new technologies implemented in current missions (Landsat 8) and future missions, including the hyperspectral infrared imager and the German satellite EnMAP [4]. End of mission is projected for late 2016 due to a local equatorial crossing time earlier than 8 A.M.

Hyperion has been used widely for a number of different studies [4] with recent examples including mapping of land-cover land-use change [5], [6]; disturbances [7]; volcanoes and geology [8], [9]; water resources [10]; evaluating seasonal dynamics at pseudoinvariant calibration sites (PICSs) and vegetated eddy covariance sites [11]; algorithm evaluations [12], [13]; and many more uses not mentioned here. The utility of Hyperion for cross-calibration has gained interest in recent mission years [14], [15] and archived data could be useful for many years to come. To show Hyperion's lifetime data record can be put on a common scale for use in these applications, a need exists to characterize orbital precession impacts to products in the latter EO-1 operational years (2011–2016). A number of recent studies have used Hyperion for cross-calibration. For example, Angal *et al.* [16] used Hyperion to cross-calibrate Landsat 7 with the Terra satellite's moderate-resolution imaging spectroradiometer (MODIS) data at the Committee on Earth Observing Satellites' Libya-4 PICS, finding that top-of-atmosphere (TOA) spectral reflectances were consistently within 7%. Angal *et al.* [15] also used Hyperion to cross-calibrate Landsat 5, Landsat 8, and Aqua MODIS TOA reflectance to within 4%. Mishra *et al.* [14] used Hyperion data to extend a cross-calibration model through visible and near-infrared (VNIR) wavelengths for the Landsat 7 Enhanced Thematic Mapper + and found accuracies of 3% with an uncertainty of $\sim 2\%$. These studies incorporated Hyperion's narrow-band VNIR and shortwave infrared (SWIR) spectrum to improve cross-calibration estimates among other satellite sensors. Estimating precession effects will be useful to other

Manuscript received February 22, 2016; revised August 10, 2016; accepted September 18, 2016. Date of publication October 13, 2016; date of current version December 7, 2016.

C. S. R. Neigh, J. McCorkel, and E. M. Middleton are with the Biospheric Sciences Laboratory, NASA Goddard Space Flight Center, Greenbelt, MD 20771 USA (e-mail: christopher.s.neigh@nasa.gov; joel.mccorkel@nasa.gov; elizabeth.m.middleton@nasa.gov).

P. K. E. Campbell is with the Joint Center for Earth Systems and Technology, University of Maryland, NASA Goddard Space Flight Center, Greenbelt, MD 20771 USA (e-mail: petya.campbell@nasa.gov).

L. Ong is with the Science Systems and Applications, Inc., NASA Goddard Space Flight Center, Greenbelt, MD 20706 USA (e-mail: lawrence.ong@nasa.gov).

V. Ly is with the Ground Software Systems Branch, NASA Goddard Space Flight Center, Greenbelt, MD 20771 USA (e-mail: vuong.ly@nasa.gov).

D. Landis is with Global Science and Technology, Inc., NASA Goddard Space Flight Center, Greenbelt, MD 20771 USA (e-mail: david.r.landis@nasa.gov).

Color versions of one or more of the figures in this letter are available online at <http://ieeexplore.ieee.org>.

Digital Object Identifier 10.1109/LGRS.2016.2612539

1545-598X © 2016 IEEE. Personal use is permitted, but republication/redistribution requires IEEE permission. See http://www.ieee.org/publications_standards/publications/rights/index.html for more information.

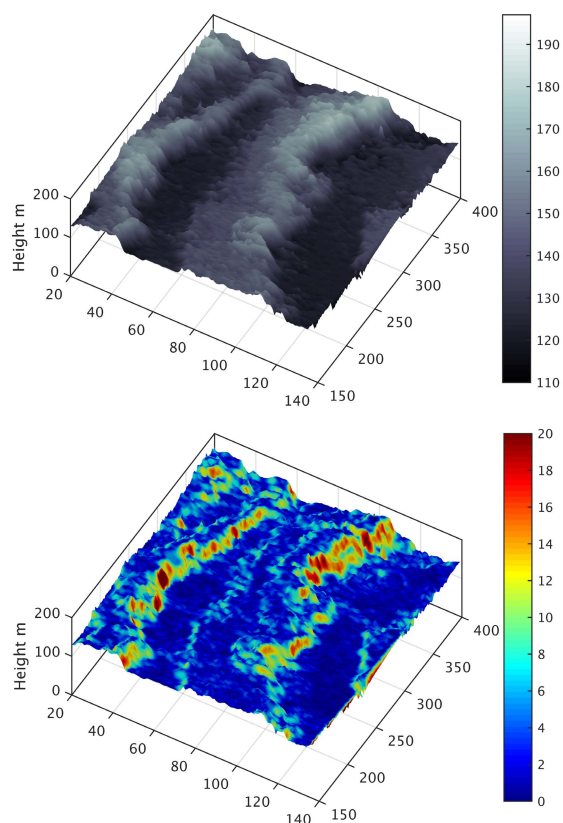


Fig. 1. Subsets of the study area shown in 3-D. (Top) WV-1 and 2 derived DTM. (Bottom) Slope estimates from DTM draped on DTM.

earth observing missions reaching end of life, as they could degrade in a similar manner.

Libya-4 is a part of the Sahara Desert, commonly referred to as the “seas of sand” (see [3, Fig. 1]) located from 28.45° to 28.65° N to 23.3° to 23.5° E, and has a mean terrain height of 113 m above sea level. Typically, aerosol loading and frequency of cloud cover are low, making it an ideal location for cross comparing earth-observing sensors. Many large irregular north-to-south dunes transect the region, with some ridges >70 m in height (Fig. 1). Govaerts [17] used the Advanced Spaceborne Thermal Emission and Reflection Radiometer global digital elevation model in Raytran (3-D radiative transfer model) simulations and concluded that the dune size and orientation can produce bidirectional distribution function (BRDF) effects from seasonal solar zenith angle and azimuth angles changes. Dune peaks can also have higher surface reflectance originating from sand properties related to grain size, shape, and composition [18], [19]. Even with these large dunes, Helder *et al.* [20] found Libya-4 to be one of the best cross-calibration sites due to high reflectance throughout the visible and SWIR (VSWIR) spectrum, with a temporal variability of <2.3% from 48 multispectral radiometrically corrected (Level 1R) Landsat 5 images. Bhatt *et al.* [21] found Libya-4 to be temporally stable within 1% and to exhibit homogeneity (SD, 1.4%) over a decade, as viewed with Aqua MODIS TOA band-1 reflectance (band center 0.65 μm , 250 m resolution). These results suggest Libya-4 is an ideal location to monitor the impacts of orbital precession on Hyperion data products. Other studies have examined the Hyperion TOA

VSWIR temporal trend in the Libya-4 PICS and found it to be stable within 2.5%–5% in most spectral bands [22]. However, this is the first study, to our knowledge, to examine Hyperion’s surface reflectance trends associated with EO-1’s rapid orbit degradation years (2013+).

We examined the impacts of orbital precession on the quality of Hyperion VSWIR spectra at the Libya-4 calibration site, for which we had three following questions.

- 1) What is the impact of orbital precession estimated with three atmospheric correction models, and are the results similar?
- 2) How spatially variable are estimates associated with large sand dunes, and how do they impact temporal trends?
- 3) Can Hyperion data (2004–2015) be used for cross-calibration?

II. METHODS AND DATA PROCESSING

A. Hyperion

In 2011, EO-1 ran out of maneuvering fuel and its orbit continued to degrade. To monitor orbital precession, we acquired near-nadir ($\pm 10^\circ$) Hyperion 30 m \times 30 m level 1 radiance images to minimize the BRDF effects from large dunes [3], [17]. Hundreds of overlapping Hyperion images are available for the Libya-4 PICS (path 181 row 40) but we used view zenith angle, solar zenith angle seasonality (May–September), and cloud screening to select 35 near-nadir images for analysis (Table I). Hyperion data were not corrected for stripping (detector gains, biases, spectral response functions, nonlinearities, noise, etc.) [23]. We applied three atmospheric correction routines, including atmospheric removal program (ATREM) [24], atmospheric correction now (ACORN) [25], and fast line-of-sight atmospheric analysis of spectral hypercubes (FLAASH) [26] using the standard parameters for the Libya-4 PICS with no spectral polishing. ATREM uses a radiation transport (RT) model based on 6S. ACORN and FLAASH are based on more complex RT models that retrieve atmospheric properties from bands near absorption features [27], [28]. Both ACORN and FLAASH, accounted for the cross-track spectral calibration variation, smile and key stone effects, with RT calculations and measured calibrated radiance data to achieve a subset of the atmospheric effects present in hyperspectral data. The derived atmospheric properties are used in conjunction with modeled atmospheric properties to correct data. All the three models use one target location within the image, therefore, in a diverse terrain the reflectance estimates are most accurate closer to the specified location. These RT approaches account for differences in the measured upwelling radiance associated with differences in solar irradiance due to different acquisition dates and times. More model information is provided in [26] and [29], and the parameters were consistently applied through time. Model versions used were 3.1, 6.1 and 1.45 for ATREM (AT), ACORN (AC) and FLAASH(F) respectively, with mid Latitude Summer seasonality.

Hyperion surface reflectances were coregistered to a Global Land Survey Landsat 8 Level 1 terrain corrected image, using

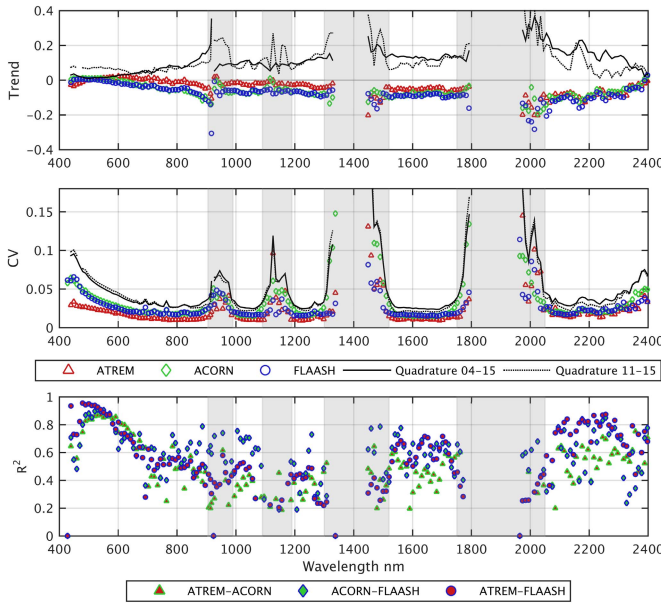


Fig. 2. Mean surface reflectances for 172 VSWIR calibrated Hyperion bands for imagery of Libya-4 acquired from 2004 through the summer of 2015. Mean lifetime trends determined with three atmospheric correction models ATREM, ACORN, and FLAASH were evaluated. (Top) Temporal trend means across the spectrum, with the Q uncertainty estimate. (Middle) CV for temporal trend, with the Q . (Bottom) Coefficient coefficient of determination (R^2) between pairs of atmospheric correction models $p < 0.01$ in all the cases.

the Environment for Visualizing Images software. More than 25 tie points were collected per image and the maximum tie-point root-mean-square error (RMSE) was 0.6 of a pixel. We subset the imagery to a consistent area overlapping high spatial resolution WorldView (WV) satellite data, located at the central lower left portion of the Hyperion image strip. We estimated the combined atmospheric model uncertainty using a quadrature (Q) statistic [30], expressed as the square root of the coefficient of variation (CV) of the sum of squares from AT, AC, and F described in

$$Q = \sqrt{AT_{cv}^2 + AC_{cv}^2 + F_{cv}^2}. \quad (1)$$

Surface reflectance coefficient of determinations (R^2 , $p < 0.01$) were also calculated as pairwise combinations between models.

B. Terrain Geometry From WorldView-1 and WorldView-2

WV data were obtained through a license agreement that the National Geospatial Intelligence Agency established with DigitalGlobe [31]. The temporal and stereoscopic satellite geometry match of August 11, 2012 for WV-1 and WV-2 provided the opportunity to produce a digital terrain model (DTM) from the 0.5-m resolution panchromatic bands allowing estimation of the impact of terrain height and slope. More details about how this DTM was processed is available in [3]. This resulted in a sample consisting of 9.7×10^4 pixels for analysis through 35 time steps.

III. RESULTS AND DISCUSSION

A. Hyperion Trend Analysis

Our results appear consistent with other studies that found Hyperion TOA reflectances to be stable within 5% in the VNIR and 10% in the SWIR [22] from 2004 through the summer of 2015. Fig. 2 displays trends, CV, and R^2 (p -val < 0.01) for reflectance in 172 calibrated bands retrieved with AT, AC, and F models. VNIR reflectance from the AT model showed small ($< 2\%$) reductions and was nearly identical to the AC or F models, and showed a slightly larger trend reduction ($\sim 10\%$) at all but a few wavelengths at the edge of atmospheric features, especially for the AC model [Fig. 2 (top)]. Trend values in the SWIR region were closer among the models, except for the F model at wavelengths < 2050 nm. This difference in reflectance retrievals among models produced variable Q uncertainties across the spectrum. Based on the AT model alone, a smaller uncertainty would be computed for this desert site. The CVs for reflectance computed from all the three models for the entire study duration were similarly low ($< 5\%$) for most wavelength regions (e.g., 450–900 nm; 1500–1800 nm; and 2050–2400 nm) except for wavelengths at the edges of atmospheric features where variable F model values were higher, contributing to a higher Q for the CVs at those wavelengths [Fig. 2 (middle)]. For the precession period, Q was greater in the VIS and less in the SWIR for trends and CVs. RT models account for differences in solar irradiance, producing apparent reflectance, and hence reducing the impact of precession. The strongest pair of correspondence between the models throughout the VSWIR was AC versus F and AT versus F models, with some of the strongest correspondence for reflectance retrievals for AT versus F models in the VIS and SWIR [Fig. 2 (bottom)].

The trends through time were examined for the mean surface reflectance retrievals for 24 evenly randomly distributed wavelengths obtained with the three models (Fig. 3). The temporal anomaly trend was low ($< \sim 5\%$) for most of these models and bands. We did not find any significant or rapid degradation from 2011 through the summer of 2015 in any product. This is expressed in the flat trends (slope of regression line ≈ 0) through time for all the examined wavelengths. Hyperion signal-to-noise ratio was originally ~ 150 in the VIS and < 110 in the SWIR [2], [26], and is declining with an earlier overpass time. Yet, the earlier overpass time reduced surface reflectance by $< 10\%$, because the models account for a reduced solar energy. Narrow-band RT models accounted for solar irradiance differences by computing: 1) reflectance as a percentage of incoming solar radiation; 2) effects of changes in the satellite–Sun geometry due to different acquisition dates and times; and 3) atmospheric properties, i.e., two-way transmittance and scattering [28], [32]–[34]. Due to this, TOA reflectance could have a larger trend.

B. WorldView DTM

To understand the impacts of large dunes on surface reflectance trends we used the WV-derived DTM to group data by dune slope ranging from 0° to 40° , and disparate areas for cross-calibration were found. Our comparison analysis

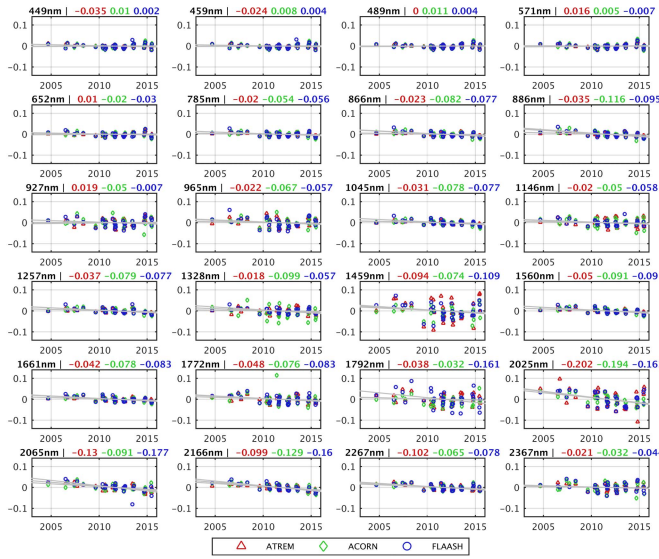


Fig. 3. Time series of the VSWIR surface reflectance anomaly trends for the study area mean from 2004 to 2015 for the three atmospheric correction models (AT, AC, and F) in 24 selected bands. The temporal trend is flat (slope ≈ 0 , $p < 0.01$) in all the cases.

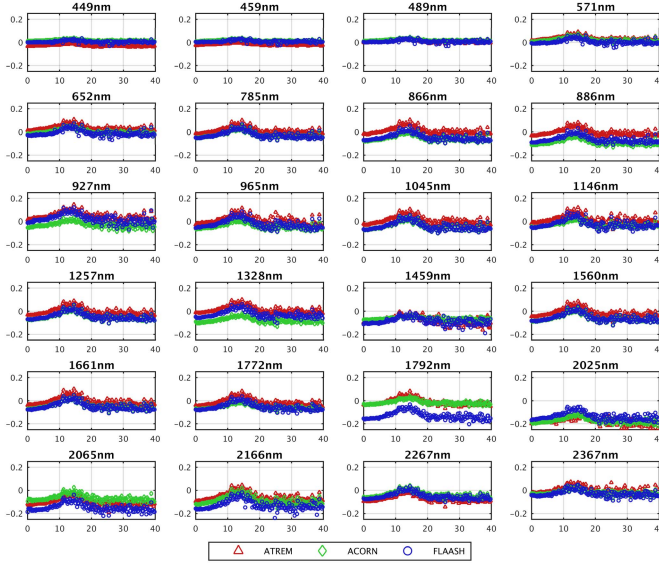


Fig. 4. VSWIR surface reflectance anomaly trends by DTM slope (0° – 40°) obtained from three atmospheric correction models (AT, AC, and F) in 24 selected bands. The most consistent results were observed for slopes $< 10^{\circ}$.

correlated surface reflectance models on a per-pixel basis in 0.05° slope increments, excluding trends with p -val < 0.01 . When Hyperion viewed dune regions associated with different degrees of slope (0° – 40°), there were noticeable differences among the three atmospheric correction models in the NIR and SWIR wavelengths, and the most consistent retrievals were made in relatively flat regions ($\sim 0^{\circ}$ – 10° slope). At slope angles $> 15^{\circ}$, a peak value in the anomaly trend was observed at many wavelengths. The results for the same 24 selected bands show that the spatial variability of the dune peaks is higher than dune flats (Fig. 4). Trends for these bands progressively increased up to 15° , then became highly variable, oscillating 2%–5% in the VIS and $> 20\%$ in the SWIR. This is because Hyperion imaged both the illuminated and

shaded portions of steep dune ridges through time, for which the illuminated versus shaded proportions varied depending upon the satellite viewing geometry. We found steep ridges illuminated from the West typically had positive trends while steep ridges from the East had negative trends. This could also be due to instrument detector and model product differences.

C. Impacts to LSI Cross-Calibration Techniques

Our study identified spatial, temporal, and spectral differences within the Libya-4 PICS. We attempted to minimize other issues that included the following.

- 1) Coregistration error between products was minimized by identifying identical points in Hyperion data, but selecting identical features distributed throughout the images was difficult in dunes. We estimate this error to be minimal (RMSE 0.6 pixels).
- 2) The seasonal BRDF effects between images were reduced but not completely ameliorated due to the differences in the image acquisition time and viewing geometry.
- 3) Degradation of Hyperion detectors was low (3%–5%) and well understood from lunar measurements [35]. Calibration coefficients were provided with “at launch” conditions, and images were not destripped.
- 4) The WV DTM defined our study area that occurred toward the center of the Hyperion swath on the image edge. This position within the swath could limit our assessment of cross-calibration due to detector differences by an unknown amount.

Our results suggest that Hyperion is stable in most bands ($< 5\%$ VNIR, and $< 10\%$ SWIR) from 2004–2015 in the Libya-4 PICS. Our results have implications for cross-calibration modeling approaches that use the Libya-4 PICS at a moderate 30 m resolution. The approaches that require a time series to minimize the BRDF error could instead use VSWIR information from Hyperion in dune flats to reduce errors in satellite sensor cross-calibration efforts.

IV. CONCLUSION

When using Hyperion surface reflectance products for cross-sensor calibration, pixels used should be coregistered and sub-sampled to specific flat portions of the site to reduce sand dune BRDF impacts. These results are similar to results from [3], and to modeled results from [17], but are here confirmed through a time series. Using dune flats could improve the possibilities of developing a robust cross-calibration model.

We had three primary questions in this paper and provide the following answers.

- 1) What is the impact of orbital precession with three atmospheric correction models, and are the results similar? We found when averaged over our study site and between reflection retrieval models in Q , Hyperion in most bands had a $< 5\%$ negative VNIR and a $< 10\%$ SWIR trend.
- 2) How spatially variable are model estimates associated with large sand dunes and how do they impact temporal trends? Trend estimates in most bands for each

atmospheric correction approach have a CV up to $\sim 5\%$ in the VSWIR and most bands have a CV $< 2.5\%$. The greatest CV is near the atmospheric absorption features and are spatially located on steep eastern dune ridges. CV for each model is greatest near these features and propagates into Q .

- 3) Can Hyperion data be used for cross-calibration? Even with variability introduced from precession, and other factors, Hyperion's spectral coverage and derived surface reflectance products remain a useful tool for land surface characterization and cross-calibration.

We suggest that future studies consider impacts of large dunes in PICS and quantify surface reflectance estimates with techniques that we applied characterizing EO-1 Hyperion precession. We also demonstrate that Hyperion data through 2015 remain a useful tool for cross-calibration.

ACKNOWLEDGMENT

The authors would like to thank the EO-1 science team for comments that improved the quality of this letter. Use of trade names is intended for clarity only and does not constitute an endorsement of any product or company by the federal government.

REFERENCES

- [1] M. A. Folkman, J. Pearlman, L. B. Liao, and P. J. Jarecke, "EO-1/Hyperion hyperspectral imager design, development, characterization, and calibration," *Proc. SPIE*, vol. 4151, p. 40, Feb. 2001.
- [2] R. O. Green, B. E. Pavri, and T. G. Chrien, "On-orbit radiometric and spectral calibration characteristics of EO-1 Hyperion derived with an underflight of AVIRIS and *in situ* measurements at Salar de Arizaro, Argentina," *IEEE Trans. Geosci. Remote Sens.*, vol. 41, no. 6, pp. 1194–1203, Jun. 2003.
- [3] C. S. R. Neigh, J. McCorkel, and E. M. Middleton, "Quantifying Libya-4 surface reflectance heterogeneity with WorldView-1, 2 and EO-1 Hyperion," *IEEE Geosci. Remote Sens. Lett.*, vol. 12, no. 11, pp. 2277–2281, Nov. 2015.
- [4] E. M. Middleton *et al.*, "The earth observing one (EO-1) satellite mission: Over a decade in space," *IEEE J. Sel. Topics Appl. Earth Observ. Remote Sens.*, vol. 6, no. 2, pp. 243–256, Apr. 2013.
- [5] R. George, H. Padalia, and S. P. S. Kushwaha, "Forest tree species discrimination in western Himalaya using EO-1 Hyperion," *Int. J. Appl. Earth Observ. Geoinf.*, vol. 28, pp. 140–149, May 2014.
- [6] A. Bannari, K. Staenz, C. Champagne, and K. S. Khurshid, "Spatial variability mapping of crop residue using Hyperion (EO-1) hyperspectral data," *Remote Sens.*, vol. 7, pp. 8107–8127, Jun. 2015.
- [7] G. Mallinis, G. Galidaki, and I. A. Gitas, "A comparative analysis of EO-1 Hyperion, Quickbird and Landsat TM imagery for fuel type mapping of a typical Mediterranean landscape," *Remote Sens.*, vol. 6, pp. 1684–1704, Feb. 2014.
- [8] A. B. Pour, M. Hashim, and J. van Genderen, "Detection of hydrothermal alteration zones in a tropical region using satellite remote sensing data: Bau goldfield, Sarawak, Malaysia," *Ore Geol. Rev.*, vol. 54, pp. 181–196, Oct. 2013.
- [9] A. G. Davies *et al.*, "Observing Iceland's Eyjafjallajökull 2010 eruptions with the autonomous NASA volcano sensor Web," *J. Geophys. Res.-Solid Earth*, vol. 118, pp. 1936–1956, May 2013.
- [10] A. Ozdemir and U. M. Leloglu, "Bathymetry and water quality measurement of shallow waters using Hyperion: Serçin lake," in *Proc. 22nd Signal Process. Commun. Appl. Conf. (SIU)*, 2014, pp. 2023–2026.
- [11] P. K. E. Campbell *et al.*, "EO-1 Hyperion reflectance time series at calibration and validation sites: Stability and sensitivity to seasonal dynamics," *IEEE J. Sel. Topics Appl. Earth Observ. Remote Sens.*, vol. 6, no. 2, pp. 276–290, Apr. 2013.
- [12] M. K. Pal and A. Porwal, "A local brightness normalization (LBN) algorithm for destriping Hyperion images," *Int. J. Remote Sens.*, vol. 36, no. 10, pp. 2674–2696, 2015.
- [13] J.-C. Thelen, S. Havemann, and G. Wong, "Surface retrievals from Hyperion EO1 using a new, fast, 1D-Var based retrieval code," *Proc. SPIE*, vol. 9472, p. 947218, May 2015.
- [14] N. Mishra, D. Helder, A. Angal, J. Choi, and X. Xiong, "Absolute calibration of optical satellite sensors using Libya 4 pseudo invariant calibration site," *Remote Sens.*, vol. 6, no. 2, pp. 1327–1346, Feb. 2014.
- [15] A. Angal, N. Mishra, X. Xiong, and D. Helder, "Cross-calibration of Landsat 5 TM, and Landsat 8 OLI with Aqua MODIS using PICS," *Proc. SPIE*, vol. 9218, p. 92180K, Sep. 2014.
- [16] A. Angal, X. Xiong, A. Wu, G. Chander, and T. Choi, "Multitemporal cross-calibration of the terra MODIS and Landsat 7 ETM+ reflective solar bands," *IEEE Trans. Geosci. Remote Sens.*, vol. 51, no. 4, pp. 1870–1882, Apr. 2013.
- [17] Y. M. Govaerts, "Sand dune ridge alignment effects on surface BRF over the Libya-4 CEOS calibration site," *Sensors*, vol. 15, no. 2, pp. 3453–3470, 2015.
- [18] G. V. G. Baranoski, B. W. Kimmel, T. F. Chen, E. Miranda, and D. Yim, "Effects of sand grain shape on the spectral signature of sandy landscapes in the visible domain," in *Proc. Int. Geosci. Remote Sens. Symp. (IGARSS)*, Melbourne, VIC, Australia, Jul. 2013, pp. 3060–3063.
- [19] H. Besler, *The Great Sand Sea in Egypt: Formation, Dynamics and Environmental Change—A Sediment-Analytical Approach*. Amsterdam, The Netherlands: Elsevier, 2008.
- [20] D. L. Helder, B. Basnet, and D. L. Morstad, "Optimized identification of worldwide radiometric pseudo-invariant calibration sites," *Can. J. Remote Sens.*, vol. 36, no. 5, pp. 527–539, Oct. 2010.
- [21] R. Bhatt, D. R. Doelling, D. Morstad, B. R. Scarino, and A. Gopalan, "Desert-based absolute calibration of successive geostationary visible sensors using a daily exoatmospheric radiance model," *IEEE Trans. Geosci. Remote Sens.*, vol. 52, no. 6, pp. 3670–3682, Jun. 2014.
- [22] T. J. Choi, X. Xiong, A. Angal, G. Chander, and J. J. Qu, "Assessment of the spectral stability of Libya 4, Libya 1, and MAURITANIA 2 sites using earth observing one Hyperion," *J. Appl. Remote Sens.*, vol. 8, no. 1, p. 083618, Jun. 2014.
- [23] L. X. Sun, R. Neville, K. Staenz, and H. P. White, "Automatic destriping of Hyperion imagery based on spectral moment matching," *Can. J. Remote Sens.*, vol. 34, no. 1, pp. S68–S81, 2008.
- [24] B. C. Gao, K. B. Heidebrecht, and A. F. H. Goetz, "Derivation of scaled surface reflectances from aviris data," *Remote Sens. Environ.*, vol. 44, nos. 2–3, pp. 165–178, May-Jun. 1993.
- [25] *ACORN User's Guide Stand Alone Version*, "A Imaging, LLC Geophysics - Analytical Imaging and Geophysics LLC," 2001.
- [26] F. A. Kruse, J. W. Boardman, and J. F. Huntington, "Comparison of airborne hyperspectral data and EO-1 Hyperion for mineral mapping," *IEEE Trans. Geosci. Remote Sens.*, vol. 41, no. 6, pp. 1388–1400, Jun. 2003.
- [27] F. A. Kruse, "Comparison of ATREM, ACORN, and FLAASH atmospheric corrections using low-altitude AVIRIS data of Boulder, Colorado," in *Proc. 13th JPL Airborne Geosci. Workshop*, Jet Propulsion Lab., Pasadena, CA, 2004, pp. 1–10.
- [28] B.-C. Gao and A. F. H. Goetz, "Column atmospheric water vapor and vegetation liquid water retrievals from airborne imaging spectrometer data," *J. Geophys. Res.*, vol. 95, no. D4, pp. 3549–3564, Mar. 1990.
- [29] B.-C. Gao, M. J. Montes, C. O. Davis, and A. F. H. Goetz, "Atmospheric correction algorithms for hyperspectral remote sensing data of land and ocean," *Remote Sens. Environ.*, vol. 113, no. 1, pp. S17–S24, Sep. 2009.
- [30] J. R. Taylor, *An Introduction to Error Analysis The Study of Uncertainties in Physical Measurements*. Mill Valley, CA, USA: Univ. Science, 1939.
- [31] C. S. R. Neigh, J. G. Masek, and J. E. Nickeson, "High-resolution satellite data open for government research," *EOS Trans.*, vol. 94, no. 13, pp. 121–123, Mar. 2013.
- [32] D. Tanre, B. N. Holben, and Y. J. Kaufman, "Atmospheric correction algorithm for NOAA-AVHRR products: Theory and application," *IEEE Trans. Geosci. Remote Sens.*, vol. 30, no. 2, pp. 231–248, Mar. 1992.
- [33] P. M. Teillet, "An algorithm for the radiometric and atmospheric correction of AVHRR data in the solar reflective channels," *Remote Sens. Environ.*, vol. 41, nos. 2–3, pp. 185–195, Aug./Sep. 1992.
- [34] A. Berk *et al.*, "MODTRAN cloud and multiple scattering upgrades with application to AVIRIS," *Remote Sens. Environ.*, vol. 65, no. 3, pp. 367–375, Sep. 1998.
- [35] J. McCorkel, K. Thome, and L. Ong, "Vicarious calibration of EO-1 Hyperion," *IEEE J. Sel. Topics Appl. Earth Observ. Remote Sens.*, vol. 6, no. 2, pp. 400–407, Apr. 2013.